Journal of ELECTRONIC MATERIALS, Vol. 45, No. 1, 2016
DOI: 10.1007/s11664-015-4164-z
© 2015 The Minerals, Metals & Materials Society

A Density Functional Investigation of the Structural, Elastic and Thermodynamic Properties of the Au–Sn Intermetallics

YALI TIAN,[1,2] WEI ZHOU,[1] and PING WU[1,3]

1.—Department of Applied Physics, Institute of Advanced Materials Physics, Tianjin Key Laboratory of Low Dimensional Materials Physics and Preparing Technology, Faculty of Science, Tianjin University, Tianjin 300072, People's Republic of China. 2.—Department of Applied Physics, Tianjin University of Commerce, Tianjin 300134, People's Republic of China. 3.—e-mail: pingwu@tju.edu.cn

The structural, elastic and thermodynamic properties of AuSn, $AuSn_2$, $AuSn_4$ and Au_5Sn are investigated by first-principles calculations. Through calculation, the four intermetallic compounds are all thermodynamically stable and AuSn has the largest negative formation energy. They are all ductile, anisotropic and have low stiffness. In addition, Au_5Sn is different from the others, since it is elastically unstable and possesses the highest anisotropy and hardness, mainly due to the strong Au–Au covalent bonds. Based on the quasi-harmonic Debye model, the thermodynamic properties of AuSn, such as the volume, thermal expansion coefficient, bulk modulus, Debye temperature and heat capacity with temperature variation in the range of 0–20 GPa, are obtained. The results indicate the increments of both the volume and thermal expansion coefficient with temperature become slow when the pressure is more than 10 GPa, and the bulk modulus and Debye temperature are almost constant below 100 K and then become linear decreasing as temperature increases. It is found that the influence of temperature on heat capacity is much more obvious than that of pressure.

Key words: Intermetallic, brittleness and ductility, thermodynamic properties, *ab initio* calculations

INTRODUCTION

Au–Sn solders are extensively used in microelectronic, optoelectronic and micro-electromechanical packaging due to the advantages of environmental friendliness, predominant creep resistance, high thermal and electrical conductivities, good inoxidizability and superior corrosion resistance.[1,2] The binary eutectic alloy solder, Au-20 wt.%Sn, is now the only replacement for the high melting point of lead-free-based alloy solders ranging from 280°C to 360°C.[3] Its service temperature can reach 300–310°C. The intermetallic compounds (IMCs) formed between solder and a solder pad during interfacial reaction are essential for the stability of the solder joints. Although the microstructure of the solder evolved during interfacial reaction has attracted many researchers,[4–8] few works about the mechanical properties of these Au–Sn compounds are presented in the published papers.[9–11] This possibly lies in the fact that preparation of the stoichiometric samples is difficult and the existing experimental technology is limited.

Based on the Au–Sn binary phase diagram,[1] the stable IMCs are Au_5Sn, AuSn, $AuSn_2$ and $AuSn_4$ at room temperature. The formation energy of these IMCs have been investigated by Chen et al. with a Miedema model,[12] by Misra et al. with an experimental method,[13] and also by Ghosh with an *ab initio* model.[14] In addition, a great deal of study has been dedicated to Au–Sn IMCs.[15–17] However, some results puzzled us. In Hu's work,[17] the Au_5Sn has the largest negative formation energy but it is elastically unstable. We know that the more negative the formation energy is, the more stable the

(Received March 11, 2015; accepted October 20, 2015; published online November 6, 2015)

crystal phase. If it is the most thermodynamically stable phase, can it be elastically unstable? It is well known that both the elastic and thermodynamic properties are crucial for IMCs presented at the interconnected interfaces in the microelectronic industry. However, there is no systematic research about the thermo-elastic properties of the Au–Sn system up to now. From these points of view, further studies are still necessary. Thus, a detailed investigation on the structural, elastic and thermodynamic properties for AuSn, $AuSn_2$, $AuSn_4$ and Au_5Sn is performed by first-principles density function calculations. We hope the present study can provide some additional information to the pre-existing data on the basic physical properties. To further understand the high temperature thermodynamic properties of these IMCs, the heat capacity, the thermal expansion coefficient and bulk modulus of AuSn as a prototype are computed through the quasi-harmonic Debye model.

COMPUTATIONAL DETAILS

We performed the first-principles calculations for the crystals of AuSn, $AuSn_2$, $AuSn_4$ and Au_5Sn. The original crystal structures of the four IMCs used for geometry optimization in this work are exhibited in Fig. 1. In all calculations, the Vienna *ab initio* simulation package was carried out to perform the electronic structure calculations based on the density functional theory. The generalized gradient approximation (GGA) of Perdew–Burke–Ernzerhof (PBE) was used as the exchange–correlation energy. Monkhorst–Pack k-point meshes were employed to evaluate Brillouin-zone integrations, and electronic occupancies were determined according to the Methfessel–Paxton technique with 0.1 eV smearing, the convergence threshold of total energy was set to below 5×10^{-6} eV/atom. The detailed cutoff energies and k-points in our calculations are shown in Table I. All the models are based on the experimental lattice constants shown in Table II.

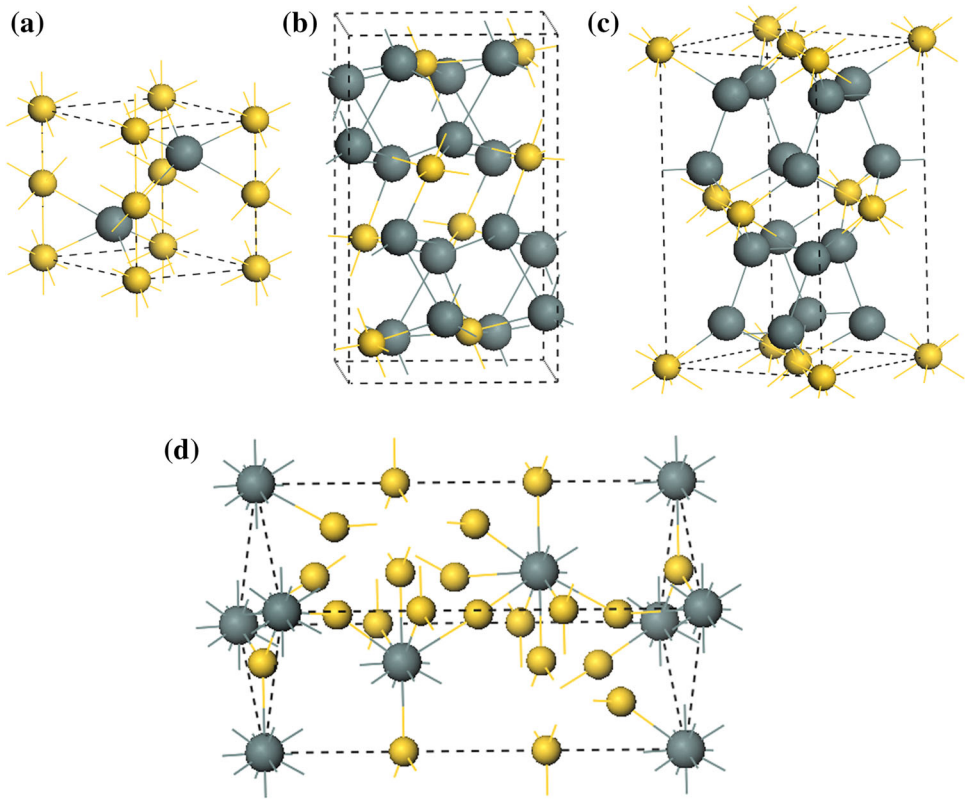

Fig. 1. Crystal structures of (a) AuSn, (b) $AuSn_2$, (c) $AuSn_4$ and (d) Au_5Sn (The grey atoms are tin and the yellow atoms are gold).

Table I. The detailed cutoff energy and k-mesh of calculations in this work

	Au	Au_5Sn	AuSn	$AuSn_2$	$AuSn_4$	β-Sn
Cut-off energy/eV	410	540	590	410	360	420
k-mesh	9 × 9 × 9	6 × 6 × 6	12 × 12 × 8	5 × 5 × 3	6 × 6 × 3	9 × 9 × 16

Table II. Crystallographic data and formation energy of Au–Sn IMCs obtained from our work and other reported values which are expressed in parentheses

Phase	Space group	Lattice constants	Formation energy (kJ/mol)
Au	225 Fm-3 m	a = 4.171 (4.078)[18]	
Au_5Sn	146 R3	a = 5.317 (5.092)[19]	−5.34 (−4.740)[14]
		c = 14.076 (14.333)	(−4.06)[13]
AuSn	194 $P6_3/mmc$	a = 4.407 (4.322)[20]	−20.31 (−18.80)[14]
		c = 5.685 (5.523)	(−21.56)[12]
			(−15.26)[13]
$AuSn_2$	61 Pbca	a = 7.03 (6.91)[21]	−16.03 (−14.40)[14]
		b = 7.15 (7.04)	(−16.53)[12]
		c = 12.10 (11.79)	(−14.2)[13]
$AuSn_4$	41 Aba2	a = 6.67 (6.51)[22]	−10.19 (−9.21)[14]
		b = 6.52 (6.52)	(−10.01)[12]
		c = 12.00 (11.71)	(−7.74)[13]
β-Sn	141 Amd	a = 5.940 (5.830)[23]	
		c = 3.213 (3.184)	

RESULTS AND DISCUSSION

Structural Properties and Formation Energy

With appropriate k-points and cutoff energy settings, the calculated lattice constants together with the available experimental values are listed in Table II. Since the exchange–correlation function GGA used in this work often overestimated the lattice constants, the calculated lattice constants have a small departure from the existing experimental values. But the differences are still in the range of allowable error. This indicates that the computational scheme applied in our work is reasonable and the calculation results are faithful.

To investigate the stability of the Au–Sn IMCs, the formation energies ΔH are computed according to the following formula:

$$\Delta H = \left[E_{\mathrm{Au}_m\mathrm{Sn}_n} - (mE_{\mathrm{Au}}(\mathrm{solid}) + nE_{\mathrm{Sn}}(\mathrm{solid}))\right]/(m+n) \quad (1)$$

In this expression, $E_{\mathrm{Au}_m\mathrm{Sn}_n}$ denotes the total energy of Au_mSn_n at the relaxed state, $E_{\mathrm{Au}}(\mathrm{solid})$ and $E_{\mathrm{Sn}}(\mathrm{solid})$ are the energies per Au atom with a face-centered cubic structure and β-Sn with a tetragonal structure in a solid state, m and n refer to the numbers of Au and β-Sn atoms in each unit cell, respectively.

The calculated results of the formation energies along with the previous experimental and theoretical values are all summarized in Table II and also plotted in Fig. 2. As shown in Fig. 2, the calculated formation energies agree well with the theoretical values from Miedema model,[12] except for Au_5Sn which has not been estimated by this mode. All of the formation energies are negative which implies that these IMCs are thermodynamically stable. Among them, the AuSn phase is the most stable one for the largest negative formation energy. While for Au_5Sn, the absolute formation energy is the lowest, corresponding to the relative inferior stability. Unfortunately, our finding is different form Hu's results.[17] In his work, it is not the AuSn, but the Au_5Sn that has the largest negative formation energy. However, the variation trend of our calculation remains in accordance with that of the experimental values[13] with a small deviation of about 1.28 kJ/mol atoms to 5.05 kJ/mol atoms. It is possible due to the fact that the experimental values are measured at room temperature while the calculations are performed at a temperature of zero. We also compare our first principles results with that of Ghosh[14] and find the difference only lies in the range of 0.61 kJ/mol atoms to 1.63 kJ/mol atoms. The minor difference is the different computational details. Specially speaking, Ghosh uses the Perdew and Wang as the exchange correlation energy while we use the PBE formalism. Although they yield a quite similar result for most materials, the PBE is most popular because it depends on both the electron density and its gradient at each space point. In addition, the cutoff energies we used are above 360 eV, higher than Ghosh's 314 eV. The consistency of these first principles calculations further proves the accuracy of our calculation scheme.

Elastic Properties

To investigate the mechanical stability of the Au–Sn IMCs, we use a stress–strain method to calculate elastic stiffness of the related phases.[24–26] The strains δ imposed on the equilibrium lattice to determine the total energy changes are less than 2%.[27] A polynomial fit of the strain energy for specific deformation is used to deduce the second-order elastic constants.[28,29] The calculated single-crystal elastic constants for the Au–Sn IMCs are displayed in Table III. The values of C_{ij} satisfy the corresponding mechanical stability rules expressed in Ref. 30, except for the Au_5Sn, as it does not con-

form to the criterion $(C_{11} - C_{12})C_{44} > 2C_{14}^2$. Thus, Au_5Sn is elastically unstable, which is consistent with Hu's results.[17]

The polycrystalline elastic modulus, such as the bulk modulus K, shear modulus G, Young's modulus E and Poisson's ratio v, can be deduced from the values of C_{ij} according to the Voight–Reuss–Hill (VRH) approximation.[25] From Table IV, the VRH Young's modulus of AuSn is 62.6 GPa, which is close to 71 GPa achieved through bulk resonance.[29] For $AuSn_4$, the VRH Young's modulus is 31.0 GPa which is close to 35.6 GPa obtained by nanoindentation of Ref. 4. For Au_5Sn, the VRH Young's modulus is 79.1 GPa which is very close to that of Chromik's work.[5] But for $AuSn_2$, the calculated value is 52.9 GPa, which is far from the experimental value of 78.3 GPa obtained with nanoindentation technique.[4] Why do not the calculation results reach good agreement with the different experimental values? There are three reasons. Firstly, the nominal stoichiometries of samples are difficult to synthesize by experiment. Secondly, the experimental Young's modulus is affected by the contact stiffness of the unloaded curve of the material. Finally, the Young's modulus is usually not the same in different directions due to the anisotropy of the bulk material. However, the calculations are based on the pure composition of the material and the same computing environment; therefore, it can give a persuasive value.

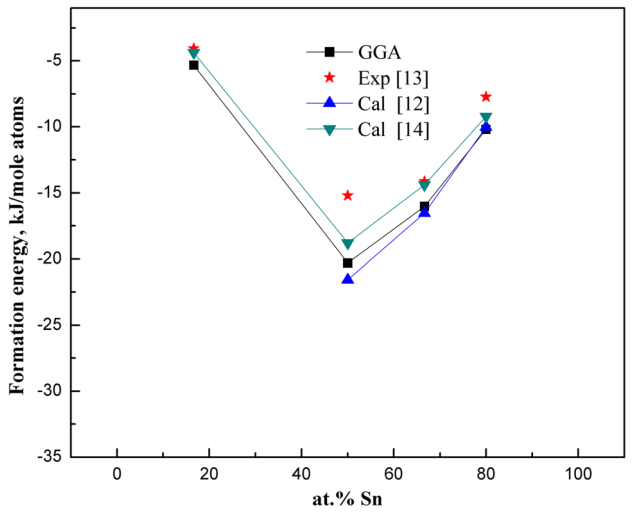

Fig. 2. Calculated formation energy compared with experimental and other theoretical values for the Au–Sn IMCs.

Pugh proposed that the quotient of the shear modulus to bulk modulus of crystalline phases, K/G, can depict the fracture ranges of the solid.[33] A high value of K/G is relevant to good ductility, and, conversely, a low value is associated with brittleness, the critical value of which is about 1.75. The values of K/G for the Au–Sn system are also listed in Table IV. We note that the K/G values are all higher than 1.75, so the Au–Sn IMCs are all ductile materials. Among them, $AuSn_4$ is the most ductile phase. In addition, the Poisson's ratio v, usually ranging from 0.25 to 0.5,[34] is a flag of the bonding force for the IMCs. The larger the Poisson's ratio is, the better the plasticity is. For the Au–Sn IMCs, the calculated Poisson's ratio of AuSn, $AuSn_2$, $AuSn_4$, Au_5Sn are 0.36, 0.35, 0.40 and 0.38, respectively. Thus, $AuSn_4$ is the one possessing the best plasticity. However, $AuSn_2$ is the owner of the weakest plasticity due to the smallest Poisson ratio. Both the ductile and plastic properties of these IMCs rank as the sequence of $AuSn_4 > Au_5Sn > AuSn > AuSn_2$. This means K/G and v have the same potency in estimating the ductile and plastic properties of the materials.

The Zener anisotropy factor, A_Z, is widely used to quantitatively analyze the degree of elastic anisotropy in a crystal. Here, we use the expression of $A_Z = \frac{2C_{44}}{C_{11}-C_{12}}$ to estimate the anisotropy of the Au–Sn system since it is successfully used in a non-cubic crystal system.[35,36] When $A_Z = 1$ it means the nanostructure is an isotropic material; otherwise it would be an anisotropic material. From the outcome shown in Table IV, the Au–Sn IMCs are all anisotropic materials and the single-crystal Au_5Sn has much a higher degree of elastic anisotropy than the others.

To further investigate the stiffness of the Au–Sn IMCs, the micro hardness parameter H[36] is also calculated in Table IV. The present value of micro hardness for AuSn, 2.14 GPa, is in agreement with the reported experimental result of 2.1 ± 0.2 GPa through micro-indentation.[37] As for $AuSn_2$ and $AuSn_4$, the computed results are 1.93 GPa and 0.70 GPa, respectively, which is close to the values obtained by the Vickers technique of 2.18 ± 0.04 GPa[38] and 0.63 ± 0.06 GPa,[39] respectively. For Au_5Sn, the calculated value of 2.3 GPa is also in the range of 2.5 ± 0.2 GPa which is the experi-

Table III. Calculated elastic stiffness (C_{ij}) of the Au–Sn IMCs

Phase	C_{11}	C_{22}	C_{33}	C_{44}	C_{55}	C_{66}	C_{12}	C_{13}	C_{14}	C_{15}	C_{23}
AuSn	95.3	–	139.1	25.6	–	–	67.4	53.4	–	–	–
$AuSn_2$	110.0	108.1	84.1	14.7	13.1	15.1	49.2	35.1	–	–	32.0
$AuSn_4$	79.5	84.4	70.5	9.2	2.3	31.9	29.1	43.2	–	–	58.7
Au_5Sn	118.6	–	178.9	36.9	–	–	92.3	106.0	24.5	–67.3	–

Table IV. The bulk modulus, shear modulus and Young's modulus including its reported value and Poisson's ratio v, Zener anisotropic factor A_z, ratio of bulk modulus to shear modulus K/G, micro hardness parameters H for the polycrystalline Au–Sn IMCs; all in GPa except for v, A_Z and K/G (dimensionless)

Phase	K	G	E		v	A_Z	K/G	H
			This work	Reported value				
AuSn	74.8	23.0	62.6	71[29] 101[30] 87[5] 50.4[31]	0.36	1.83	3.25	2.14
$AuSn_2$	59.5	19.5	52.9	103[5] 78.3[4]	0.35	0.48	3.05	1.93
$AuSn_4$	54.4	11.1	31.0	39[5] 71.1[31] 35.6[4]	0.40	0.36	4.89	0.70
Au_5Sn	109.7	28.7	79.1	62[29] 76[5] 78[32]	0.38	2.80	3.67	2.30

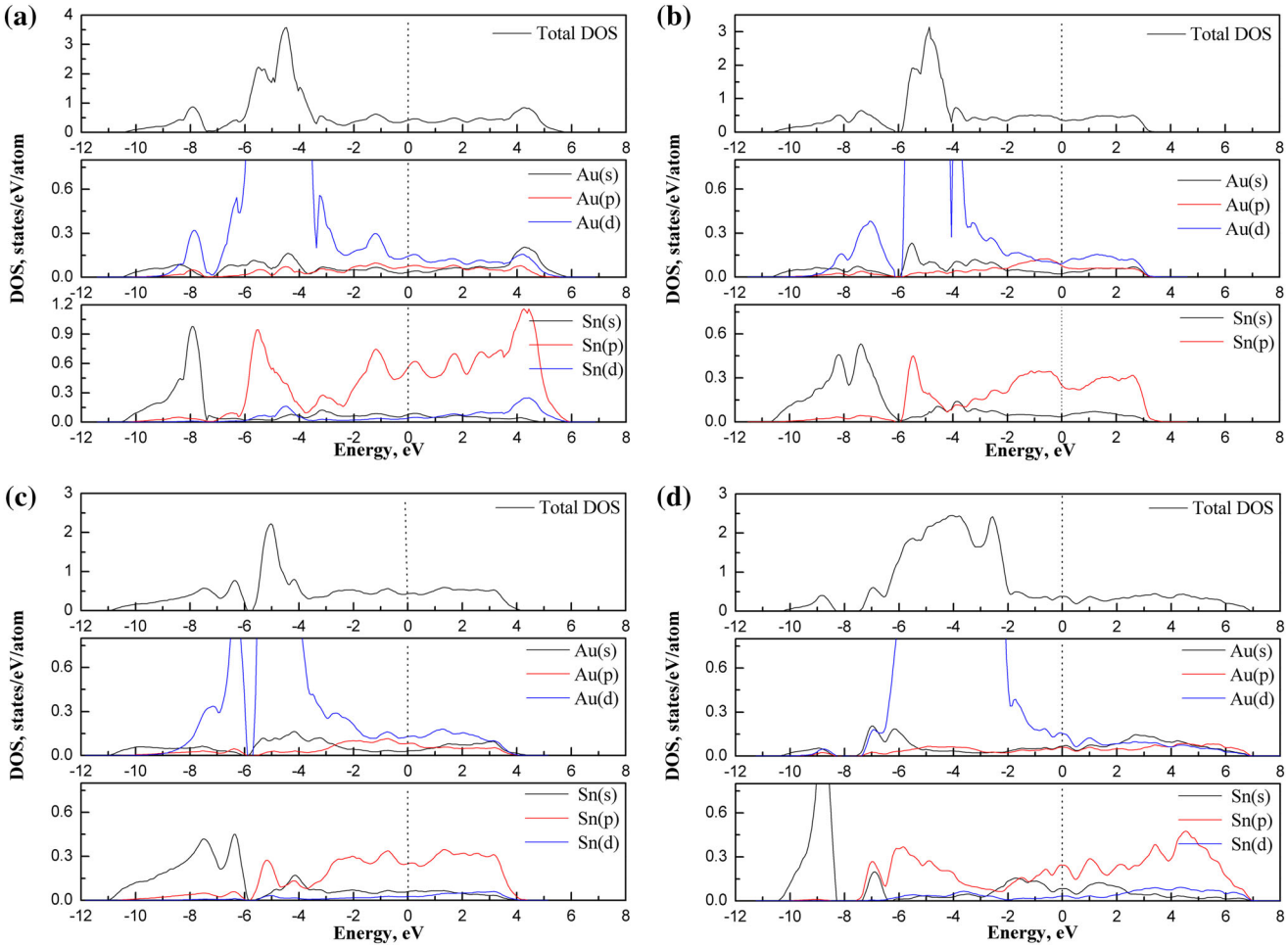

Fig. 3. The total density of state (TDOS) and partial density of state (PDOS) of (a) AuSn, (b) $AuSn_2$, (c) $AuSn_4$ and (d) Au_5Sn.

mental result obtained by nanoindentation testing.[5] These good agreements manifest that our calculation method for the elastic properties is reasonable and reliable. The calculated hardness values for the four Au–Sn IMCs indicate they are all low-stiffness materials. Au_5Sn is the one with the highest hardness while $AuSn_4$ is the lowest one among them.

Electronic Structure

To further explore the electronic state of the Au–Sn IMCs, the total electronic density of states (TDOS) together with the partial density of states (PDOS) are illustrated in Fig. 3. The four IMCs are all metallic since the electrons' densities of states at the Fermi level are non-zero. Based on the four

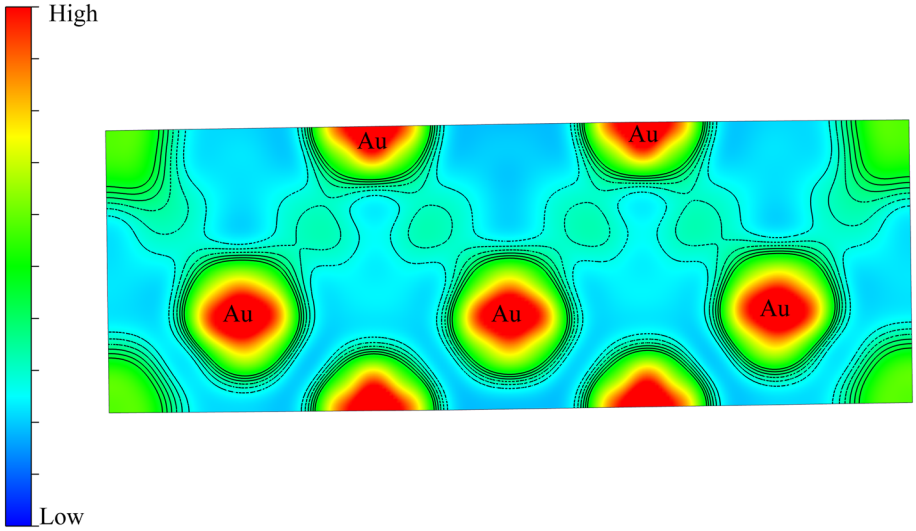

Fig. 4. Difference charge density distribution of Au_5Sn in the Au-rich plane.

TDOS values, the contribution to the DOS at the low-lying states from −10.8 eV to −7.3 eV for AuSn, −10.6 eV to −6.0 eV for $AuSn_2$ and −10.9 eV to −5.9 eV for $AuSn_4$ is mainly driven by Sn-*s* states together with Au-*d* states, indicating hybridization of Sn-*s* and Au-*d* electrons. For Au_5Sn, the contribution to the DOS from −10.5 eV to −8.2 eV is mainly dominated by the Sn-*s* state; the Au-*d* state made scarcely any contribution to the TDOS. While the contribution to the DOS from −7.3 eV to the Fermi level for AuSn, −6.0 eV to the Fermi level for $AuSn_2$ and $AuSn_4$, −7.6 eV to the Fermi level for Au_5Sn is dominated by Au-*d* states and slightly with Sn-*p* states, meaning a weak hybridization of Au-*d* and Sn-*p* electrons. Above the Fermi level, the TDOS is relatively low and flat because the majority of *d* orbits of Au are occupied. For Au_5Sn, the obvious difference from others is the broad bonding peak appearing between −7.6 eV and −1.9 eV, predominately composed by the Au-*d* state which slightly hybridized with the Sn-*p* state. Because the proportion of Au atoms is more in Au_5Sn than other Au–Sn IMCs, the interactions of Au atoms could play a leading role. The hybridization of Au-*d* with Sn-*p* states minimizes the exclusion energy between Au and Sn, forming more stable bonds. The strong interaction of Au atoms together with the orbit hybridization leads to the energy increasing which may be in agreement with the highest formation energy (namely, the lowest absolute formation energy) of Au_5Sn.

To gain further insight into the bonding characteristics in Au_5Sn, the difference charge density is analyzed in Fig. 4. Here, the electron density difference is the difference between the electron density of the bonded atom and the isolated atom, and it is helpful to visualize the electron redistribution of the atoms after chemical bonding. It is clear that significant electron density accumulates in the core region of Au atoms while it is minor around Sn atoms. There are electron densities surround the two adjacent Au atoms which signify the covalent bonding character to some degree. Based on the distribution of the DOS of Au_5Sn, Hu also pointed out the Au–Au covalent bond character because of the broad bonding peak near the Fermi level being predominately donated by the Au-*d* states.[17] We think the strong covalent bonds may be the main cause of high elastic anisotropy of Au_5Sn.

Thermodynamic Properties

The theoretical results mentioned above only give the material properties at the ground state without including thermal effects. However, the Au-20 wt.%Sn is a potential high-temperature lead-free based alloy solder, the thermal properties of which should not be neglected. Due to the experimental limit in determining the thermal properties, it is worth carrying out such calculations. There are two IMCs contained in this eutectic alloy solder, namely Au_5Sn and AuSn. AuSn is the one with higher content and more mechanical stability based on the elastic stability criteria. So, it is crucial for the thermal stability. In this work, the thermodynamic properties of AuSn with temperature variation in the range of 0–20 GPa are investigated by first-principles calculations combined with the quasi-harmonic Debye model which is described in detail by Blanco.[40,41] The third-order Birch–Murnaghan equation of state is given by the following equation[24]:

$$E = E_0 + \left(\frac{9}{16}\right)B_0V_0\left\{\left[\left(\frac{V_0}{V}\right)^{\frac{2}{3}}-1\right]^3 B_0' + \left[\left(\frac{V_0}{V}\right)^{\frac{2}{3}}-1\right]^2\left[6-4\left(\frac{V_0}{V}\right)^{\frac{2}{3}}\right]\right\} \quad (2)$$

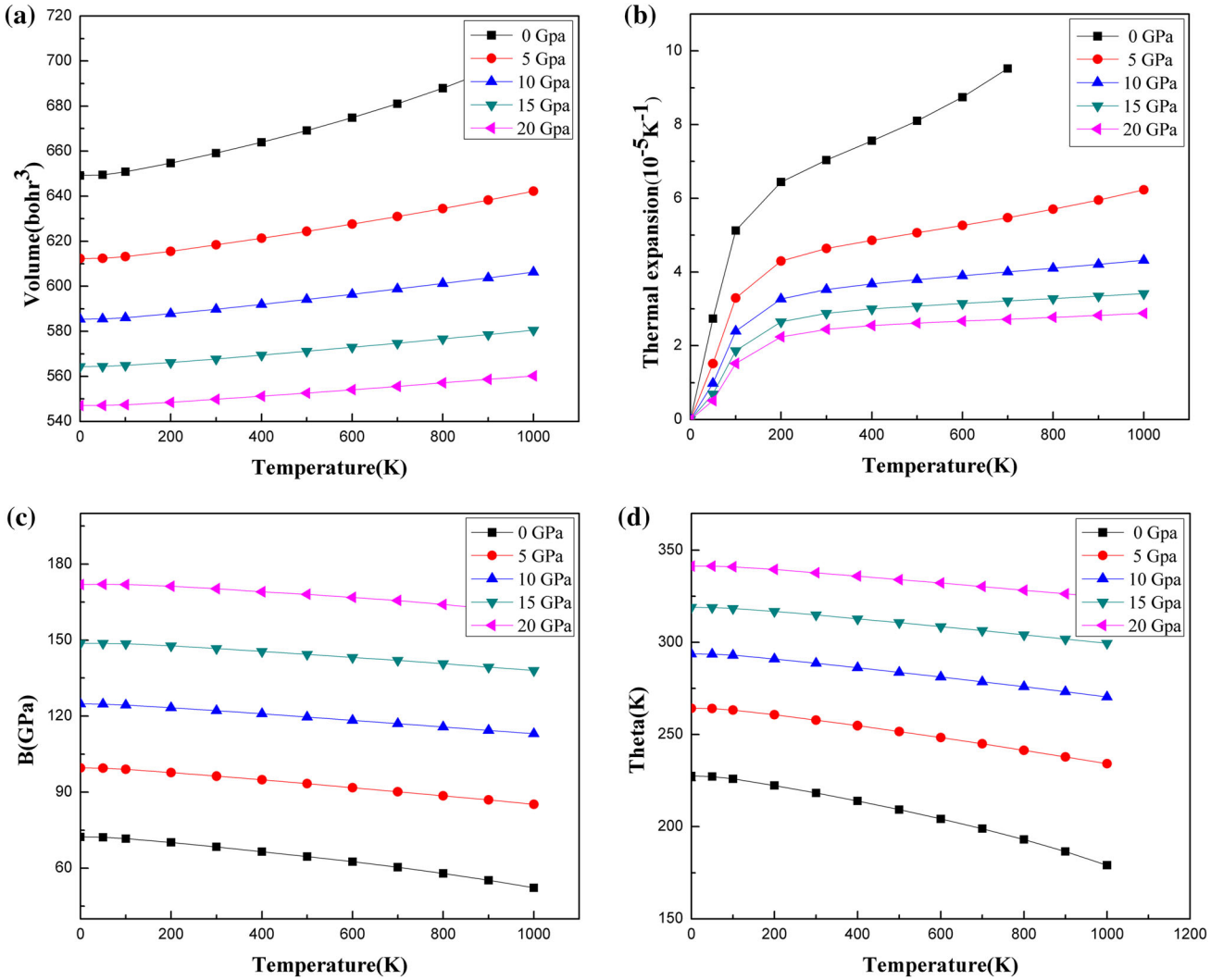

Fig. 5. The variations of (a) volume, (b) thermal expansion coefficient, (c) bulk modulus and (d) Debye temperature with temperature and pressure for AuSn.

Here V_0 and E_0 refer to the equilibrium unit cell volume and energy, respectively, B_0 is the bulk modulus and B_0' is its pressure derivative. These parameters are all equivalent to the zero-pressure and zero-temperature values.

Through computing groups of volumes around the equilibrium unit cell of AuSn together with the corresponding energy changes and fitting these data to Eq. 2, we can obtain the parameters such as V_0, E_0, B_0 and B_0'. Furthermore, applying the quasi-harmonic Debye model, we can derive the high-temperature thermodynamic properties of AuSn. Figure 5a shows the relationships of volume as a function of temperature and pressure. At a given pressure, the volume is almost a constant below 100 K. At more than 10 GPa, the rising tendency of the volume with temperature becomes slow. Variations of the volume thermal expansion coefficient α depending on temperature and pressure are presented in Fig. 5b. It can be seen that the pressure effect on the thermal expansion coefficient α below 100 K is small. At more than 100 K, the effect is increasingly apparent. For a given temperature, the thermal expansion coefficient α decreases with increasing pressure. At a given pressure, α increases sharply with temperature below 100 K. At more than 100 K, the increase rate approaches a linear mode little by little. At last, the increasing trend becomes gentler. When P > 10 GPa, the increment of α is diminishing at high temperature and the curves are almost parallel to the temperature axis. This signifies that AuSn has good properties of volume invariance under high pressure after it overcomes original and obvious volume expansion, which remains in accordance with the variation trend of volume with temperature at high pressure delineated in Fig. 5a. Comparing the α of AuSn with that of Cu_6Sn_5[42] at 300 K and 0 GPa, we have found that the former is a little higher than the latter. For example, the calculated values for AuSn and Cu_6Sn_5

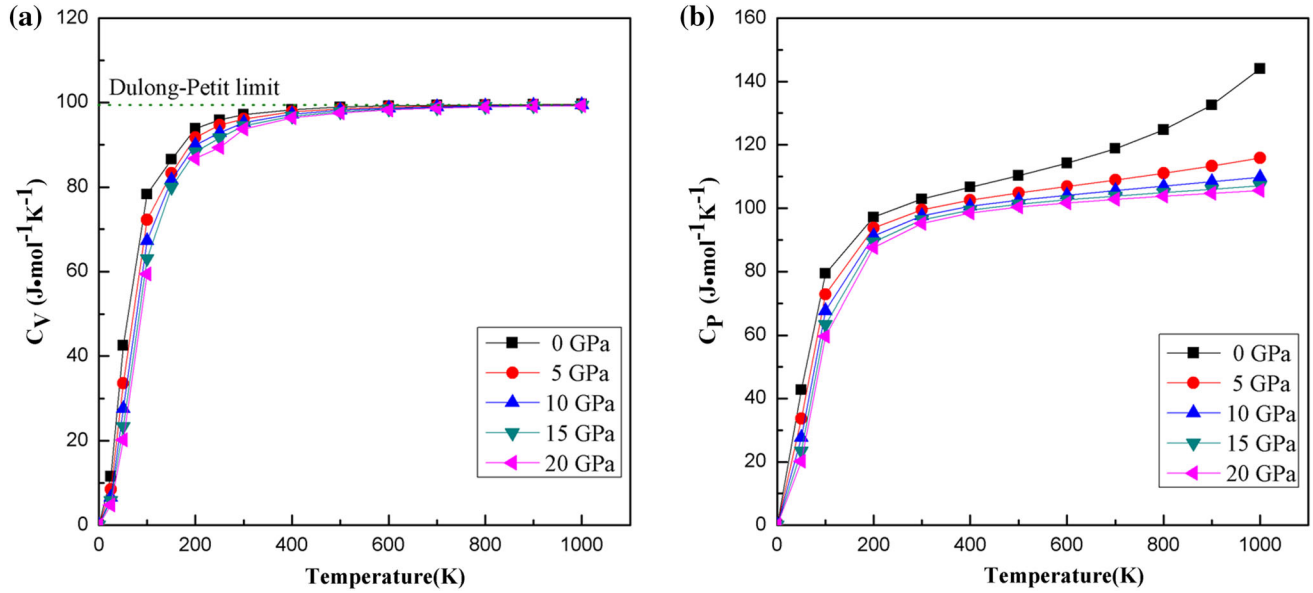

Fig. 6. The variations of (a) constant volume heat capacity C_V and (b) constant pressure heat capacity C_P with temperature in the range of 0–20 GPa for AuSn.

are 7.03×10^{-5} and 6.07×10^{-5} K^{-1}, respectively. Therefore, AuSn is more favorable to the interconnection of high-melting solder with a solder pad.

The variations of the bulk modulus B as a function of temperature from 0 K to 1000 K at different pressures (P = 0 GPa, 5 GPa, 10 GPa, 15 GPa, 20 GPa) are calculated and depicted in Fig. 5c. It is clear that both temperature and pressure affect the bulk modulus. At a given pressure, the bulk modulus is almost a constant below 100 K. At more than 100 K, it decreases linearly with temperature. When the temperature is kept constant, the bulk modulus increases with pressure. This may be attributed to the fact that due to shrinking of the crystal volume, the inter-atomic interaction force increases, which leads to the material being difficult to compress. Debye temperature θ_D is another basic thermodynamic parameter in the quasi-harmonic Debye model, which is related to the average sound velocity of the solid. Figure 5d presents the relation of θ_D with temperature and pressure. Based on the quasi-harmonic Debye model, θ_D is connected with the bulk modulus and volume. At a given pressure, the bulk modulus and volume are almost constant below 100 K, therefore, θ_D is almost constant. At more than 100 K, θ_D decreases linearly with temperature. When the temperature is given, θ_D increases with the pressure, the variation trend of which is analogous to that of the bulk modulus, as shown in Fig. 5c.

Finally, the heat capacity at constant volume C_V and heat capacity at constant pressure C_P as functions of temperature and pressure are also computed, and the results are shown in Fig. 6. When the temperature is 0 K, the heat capacity is 0, since the phonon is frozen in a ground state, being difficult to stimulate. When the temperature is above 0 K, the thermally activated phonons are increasing, so the heat capacity increases. It can be found that both of the heat capacities are proportional to T^3 at sufficiently low temperatures. However, with temperature increasing, the difference between C_V and C_P becomes more and more large. Additionally, C_V depends on both temperature and pressure below 400 K due to the anharmonic effect.[43] At higher temperatures, C_V tends to approach the Dulong–Petit classical limit [$C_V \propto 3nR = 99.77$ J/mol K, here four atoms are contained in the hexagonal structure of AuSn, see Fig. 1a] since the anharmonic effect on C_V is suppressed, but C_P still increases with temperature at a slow speed. It is obvious that the heat capacities increase with temperature at the same pressure and decrease with pressure at the same temperature. In addition, the influences of temperature on the heat capacity are much more obvious than that of the pressure on it.

We ever guessed the difference of the formation energy between our first-principles calculation and the experimental values may be due to a temperature effect. To make it clear, we estimated the difference from our heat capacity results. Take AuSn as an example. Based on the curve of C_V with temperature, we can calculate the heat absorbed by AuSn from 0 K to 298 K at 0 GPa. Thus, the total energy of AuSn at 298 K can be derived by the aforementioned heat added the energy of 0 K through our first-principles calculation. Similarly, the total energy of Au and β-Sn at 298 K can be derived. Using formula (1), we can derive the formation energy of AuSn at 298 K. We have found it is −19.85 kJ/mol atoms, slightly higher than −20.31 kJ/mol atoms at 0 K with the deviation of 0.46 kJ/mol atoms. This means the temperature would cause a little increase of the formation en-

ergy, but this effect is so insignificant that it can be neglected for AuSn from the analyses point of C_V.

CONCLUSIONS

In this work, the structural, elastic and electronic properties of Au–Sn IMCs are investigated based on the first-principles density functional and Voigt-Reuss-Hill approximation. Through calculations, we have found the Au–Sn IMCs are all stable according to the formation energies, and AuSn has the largest negative formation energy. However, Au_5Sn is elastically unstable. The values of K/G show that the Au–Sn IMCs are all ductile materials, the Poisson's ratios v manifest that they are all plastic materials. The ductile and plastic properties of these IMCs rank as follows: $AuSn_4 > Au_5Sn > AuSn > AuSn_2$. The Zener anisotropy factor A_Z shows that the Au–Sn IMCs are all anisotropic materials. The micro hardness parameters (H) indicate they are all low-stiffness materials. And Au_5Sn is the one with the highest anisotropy and hardness mainly due to the strong Au–Au covalent bonds according to the DOS and the difference charge density distribution. In addition, the thermodynamic properties of AuSn with the variation of temperature in the range of 0–20 GPa are investigated by the quasi-harmonic Debye model. Below 100 K, the volume, bulk modulus and Debye temperature are almost constant. Above 10 GPa, the increments of both the volume and thermal expansion coefficient with temperature are diminishing, and the decrements of both the bulk modulus and Debye temperature become slow. The heat capacity C_V tends to the Dulong–Petit limit at high temperature and high pressure, and the influence of temperature on the heat capacity is much more obvious than that of pressure on it. These results imply that AuSn has good structural stability and anti-pressure ability and is beneficial to the interconnection of a high-melting solder with a solder pad. All of the calculations will provide some perfect guide for the actual use of the material.

ACKNOWLEDGEMENTS

This work was supported by the National Natural Science Foundation of China (51572190), and the super computing resources were supported by the High Performance Computing Center of Tianjin University, China.

REFERENCES

1. G.S. Matijasevic, C.C. Lee, and C.Y. Wang, *Thin Solid Films* 223, 276 (1993).
2. D.G. Ivey, *Micron* 29, 281 (1998).
3. A.A. Wronkowsk, G. Czerniak, and A. Wronkowski, *Appl. Surf. Sci* 610, 161 (2014).
4. Y.K. Wang, W.S. Liu, Y.Z. Man, Y.F. Huang, Y. Tang, F. Cheng, and Q. Yu, *Mater. Sci. Eng. A* 610, 161 (2014).
5. R.R. Chromik, D.N. Wang, A. Shugar, L. Limata, M.R. Notis, and R.P. Vinci, *Mater. Res. Soc.* 20, 2161 (2005).
6. L. Zavalij, A. Zribi, R.R. Chromik, S. Pitely, P.Y. Zavalij, and E.J. Cotts, *J. Alloy. Compd.* 334, 79 (2002).
7. J.Y. Tsai, C.W. Chang, Y.C. Shieh, Y.C. Hu, and C.R. Kao, *J. Electron. Mater.* 34, 182 (2005).
8. J.W. Yoon, H.S. Chun, J.M. Koo, and H.J. Lee, *Scr. Mater.* 56, 661 (2007).
9. P. Hohenberg and W. Kohn, *Phys. Rev. B* 136, 864 (1964).
10. J.W. Yoon, H.S. Chun, B.I. Noh, and S.B. Jung, *Microelectron. Reliab.* 48, 1857 (2008).
11. X.F. Wei, Y.K. Zhang, and R.C. Wang, *Microelectron. Reliab.* 53, 748 (2013).
12. H.M. Chen and X.P. Zhong, *J. Guangxi Univ. (Nat. Sci. Ed.)* 29, 98 (2004).
13. S. Misra, B.W. Howlett, and M.B. Bever, *Trans. Met. Soc. AIME* 233, 749 (1965).
14. G. Ghosh, *J. Mater. Res.* 23, 1398 (2008).
15. C. Ghosh, *Intermetallics* 18, 2178 (2010).
16. C.E. Ho, L.C. Shiau, and C.R. Kao, *J. Electron. Mater.* 31, 1264 (2002).
17. J.Q. Hu and M.Z. Xie, *Acta Phys. Sin.* 62, 247102 (2013).
18. B.N. Dutta and B. Dayal, *Phys. Status. Solidi.* 3, 473 (1963).
19. K. Osada, S. Yamaguchi, and M. Hirabayashi, *Trans. Jpn. Inst. Met.* 15, 256 (1974).
20. J.P. Jan, W.B. Pearson, A. Kjekshus, and S.B. Woods, *Can. J. Phys.* 41, 2252 (1963).
21. K. Schubert, H. Breimer, and R. Gohle, *Z. Metallkde.* 50, 146 (1959).
22. R. Kubiak and M. Wolcyrz, *J Less Common Met.* 97, 265 (1984).
23. W.J. Helfrich and R.A. Dodd, *Acta Metall.* 12, 667 (1964).
24. Y.F. Wu, B. Wu, and Z.Y. Wei, et al., *Intermetallics* 53, 26 (2014).
25. W. Zhou, L.J. Liu, B.L. Li, and P. Wu, *Comp. Mater. Sci.* 46, 921 (2009).
26. S. Wang and H.J. Ye, *Phys. Condens. Matter* 15, 5307 (2003).
27. Gökhan Gökoğlu, *J. Phys. Chem. Solids* 69, 2924 (2008).
28. W.C. Hua, Y.A. Liu, D.J. Li, and H.L. Jin, *Comp. Mater. Sci.* 99, 381 (2015).
29. R.M. Wentzcovitch, N.L. Ross, and G.D. Price, *Phys. Earth Planet. Inter.* 90, 101 (1995).
30. J.E. Osburn, M.J. Mehl, and B.M. Klein, *Phys. Rev. B* 43, 1805 (1991).
31. F.G. Yost, M.M. Karnowsky, W.D. Drotning, and J.H. Gieske, *Metall. Mater. Trans. A* 21, 1885 (1990).
32. R. An, C.Q. Wang, and Y.H. Tian, *J. Electron. Mater.* 37, 968 (2008).
33. F. Pugh, XCII. *Philos. Mag.* 45, 823 (1954).
34. X.D. Zhang, C.H. Ying, and Z.J. Li, *Superlattice Microstruct.* 52, 459 (2012).
35. H.-C. Cheng, C.-F. Yu, and W.-H. Chen, *J. Alloy Compd.* 546, 286 (2013).
36. H.-C. Cheng, C.-F. Yu, and W.-H. Chen, *Comp. Mater. Sci.* 81, 146 (2014).
37. A. Vicenzo, M. Rea, L. Vonella, M. Bestetti, and P.L. Cavallotti, *J. Solid State Electrochem.* 8, 159 (2004).
38. J. Ciulik and M.R. Notis, Materials and Processes, in *Proceedings of the 2nd ASM International Electronic Materials and Processing Congress*, ASM International, Materials Park, 1989, pp. 57–61.
39. G. Ghosh, *J. Mater. Res.* 19, 1439 (2004).
40. M.A. Blanco, E. Francisco, and V. Luana, *Comput. Phys. Commun.* 158, 57 (2004).
41. E. Francisco, M.A. Blanco, and G. Sanjurjo, *Phys. Rev. B* 63, 094104 (2001).
42. W. Zhou, L.J. Liu, and P. Wu, *Intermetallics* 18, 922 (2010).
43. J.N. Yuan, Z.L. Lv, and Q. Lu, *Solid State Sci.* 40, 1 (2015).